HHS Public Access

Author manuscript

Mach Learn Appl. Author manuscript; available in PMC 2023 November 30.

Published in final edited form as:

Mach Learn Appl. 2023 September 15; 13: . doi:10.1016/j.mlwa.2023.100477.

Application of deep neural networks for inferring pressure in polymeric acoustic transponders/sensors

Seyedhamidreza Alaie[a,*], **Subhi J. Al'Aref**[b]

[a]Department of Mechanical & Aerospace Engineering, New Mexico State University, Las Cruces, NM, USA

[b]Department of Internal Medicine — Division of Cardiovascular Medicine, University of Arkansas for Medical Sciences, Little Rock, AR, USA

Abstract

Passive sensor-transponders have raised interest for the last few decades, due to their capability of low-cost remote monitoring without the need for energy storage. Their operating principle includes receiving a signal from a source and then reflecting the signal. While well-established transponders operate through electromagnetic antennas, those with a fully acoustic design have advantages such as lower cost and simplicity. Therefore, detection of pressures using the ultrasound signal that is backscattered from an acoustic resonator has been of interest recently. In order to infer the pressure from the backscattered signal, the established approach has been based upon the principle of detection of the shift to the frequency of resonance. Nevertheless, regression of the pressure from the signal with a small error is challenging and has been subject to research. Here in this paper, we explore an approach that employs deep learning for inferring pressure from the ultrasound reflections of polymeric resonators. We assess if neural network regressors can efficiently infer pressure reflected from a fully acoustic transponder. For this purpose, we compare the performance of several regressors such as a convolutional neural network, a network inspired by the ResNet, and a fully connected neural network. We observe that deep neural networks are advantageous in inferring pressure information with a minimal need for analyzing the signal. Our work suggests that a deep learning approach has the potential to be integrated with or replace other traditional approaches for inferring pressure from an ultrasound signal reflected from fully acoustic transponders or passive sensors.

Keywords

Pressure sensor; Neural networks; Deep learning; Ultrasound; Transponder; Passive sensor

*Corresponding author. alaie@nmsu.edu (S. Alaie).

CRediT authorship contribution statement

Seyedhamidreza Alaie: Conceived the idea, Developed the benchtop test setup, Analyzed the data, Wrote the first draft. **Subhi J. Al'Aref:** Assisted in writing the paper, Contributed during the course of this study by providing feedbacks on its potential applications and metrics applicable to medical devices.

1. Introduction

Applications of deep neural networks (NN) in the area of computerized interpretation of images and ultrasound signals are rapidly growing. Utility of deep learning in processing ultrasound signals for nondestructive testing (Haile, Zhu, Hsu, & Bradley, 2020; Zhang & Harvey, 2012), have been applied in characterization of cracks (Pyle et al., 2020), defects (Medak, Posilović, Subašić, Budimir, & Lončarić, 2022; Ye, Ito, & Toyama, 2018), weld geometries (Provencal & Laperrière, 2021), and the classification of direct/indirect reflections (Haile et al., 2020). These reports are a few examples to highlight the utility of deep learning for interpretation of ultrasound signals/images (Ye et al., 2018). Use of deep learning in ultrasound imaging (Lafci, Merčep, Morscher, Deán-Ben, & Razansky, 2020) and beam forming (Luijten et al., 2019) are other examples of the growing interest in this field. Accordingly, deep learning offers a great tool for enhancement of the current state of art approaches for interpretation of ultrasound signals.

Another area, in which deep learning has been utilized in, is interpreting backscattered electromagnetic signals from transponders (Amendola, Bianchi, & Marrocco, 2015; Shi, He, Gu, & Jiao, 2021; Zhao, Sunny, Li, & Wang, 2022). The conventional chipless passive sensors (Hennig & vom Bögel, 2010; Lin & Kao, 2008) have been demonstrated to be beneficial in situations where the use of electronics has been shown to be disadvantageous such as radiation sensors (Debourg et al., 2014), humidity (Raju & Bridges, 2021), temperature (Martínez-Martínez, Galindo-Romera, & Herraiz-Martínez, 2017), or chemical detections (Raju & Bridges, 2022). They have also been demonstrated in applications such as tagging (Lin & Kao, 2008) and pressure measurement (Nguyen, Fernandes, & Häfliger, 2014; Schimetta, Dollinger, Scholl, & Weigel, 2001). The interest in these electromagnetic transponder/sensors has led to the application of NNs and other machine learning algorithms for interpreting signals from these classes of sensors (Villa-Gonzalez, Bhattacharyya, & Sarma, 2021). While the application of NNs in interpreting signals from transponder/sensors, that operate with electromagnetic waves, has been studied; their utility for chipless acoustic transponders/sensors (Ishihara et al., 1988; Jiang et al., 2020; Tremblay-Darveau, Williams, & Burns, 2014) has been unexplored. Recent studies on the use of fully acoustic transponders/sensors that operate with shift of resonance (Li, Li, & Yan, 2018; Tremblay-Darveau et al., 2014), raise the question of how/if NN can be leveraged for inferring data from these transponder/sensors as they did with transponders operating with electromagnetic waves (Amendola et al., 2015; Shi et al., 2021; Zhao et al., 2022).

The aforementioned wide range of applications of deep learning raises the question of the utility of deep learning for inferring data from the ultrasound signals backscattered from sensors/transponders. Here to test this hypothesis we employ polymeric acoustic resonators that can deform at various pressures. This experiment is aligned with the previous reports on detecting pressure from the ultrasound reflected from various forms of microbubbles, (Forsberg et al., 2005; Ishihara et al., 1988; Li et al., 2018; Tremblay-Darveau et al., 2014), in which pressure was extracted from the resonant frequency shift due to contraction of the microbubbles at higher pressures. To test our hypothesis, we interpret the signal with conventional measurement of a resonant frequency shift (Fairbank & Scully, 1977; Ishihara et al., 1988; Sojahrood, Falou, Earl, Karshafian, & Kolios, 2015), and compare it with that of

deep neural networks. To collect the training/test datasets we fabricate and utilize a benchtop test setup that is capable of measurement of echo signal from the pressure chamber in an aqueous environment. This setup stores the fast Fourier transform (FFT) of the reflection signals at 3200 randomly selected pressures ranging from 0 to 158 mmHg. Subsequently, the dataset is used for determining the effectiveness of a NN-based approach for interpreting the pressure from the echo signals.

The interest in the estimation of pressures using deep learning raises the question about the suitable neural network architecture for regressing pressure. Inferring the information from an echo signal, especially from a polymeric sample, is challenging due to several factors. Topology of the transponder (such as buckled bubbles, Tremblay-Darveau et al., 2014), any motion of the transponder induced by the pressure, change in the dimensions induced by the pressure (Tremblay-Darveau et al., 2014), pulser's settings, and ultrasound transducer itself all can introduce multiple dips and peaks in the echo signal. It is possible to observe multiple dips/peaks, associated with a transponder/sensor, for different harmonics (e.g. in the case of microbubbles Li et al., 2018, fundamental, subharmonic and ultraharmonic). In addition, both amplitude (Li et al., 2018) and frequencies (Tremblay-Darveau et al., 2014) associated peaks/dips, have been shown to be correlated to pressure. Therefore, given the aforementioned complexities, we hypothesize that deep learning can infer pressure from multiple features (peaks' shape amplitude and overall shape) and be advantageous in processing echo signals.

In selection of a regressor architecture we considered several factors including dataset size, features expected to be influential in the datapoints, as well as the prior reports. Various architectures for regression have been presented in the literature (Ahn, Byun, Oh, & Kim, 2012; Pandey, Zakwan, Sharma, & Ahmad, 2020; Zhou, Pierre, & Trudnowski, 2011), such as those inspired by convolutional neural networks (CNNs) (Zhu, Li, Mo, & Wu, 2017) and residual neural network (ResNet) (Chen, Hu, Nian, & Yang, 2020), or fully connected (dense) network (Kohler & Langer, 2021). In this work, the dataset and the dimension of the feature vectors are relatively small therefore low-capacity models with dropout regulation are preferred. The shift in the frequency for certain dips/peaks, in an echo signal is expected to be an influential feature (Forsberg et al., 2005), which could be extracted by the convolutional layers. Accordingly, we chose a low-capacity CNN regressor, similar to prior efforts (Pyle et al., 2020) in the area of ultrasound imaging. We also expect other features such as the shape and quality factor of the peaks/dips to be influential. Moreover, the relationship between the shift to the center frequency is possible to be nonlinear. This is why we choose the ResNet Style regressor that was reported to be advantageous for nonlinear functions (Chen et al., 2020). Choosing a CNN, Baseline, and ResNet Style regressor enables extraction of the main influential features in the learning algorithm.

The primary contribution of this work is investigating if NNs could be advantageous in the application of inferring pressure from an acoustic transducer/sensor that lacks electronics. Many attempts have been made to improve the sensitivity of measurement of pressure in such systems with passive sensors being microbubbles (Forsberg et al., 2005), coated microbubbles (Li et al., 2018), microbubbles encapsulated in polymers (Ishihara et al., 1988), or imaging the dimensions of a deformable sensor (Jiang et al., 2020). Majority

of these efforts have been directed toward engineering of the uniformity/shape of acoustic resonators (Tremblay-Darveau et al., 2014), use of resonant frequency for inferring pressure (Ishihara et al., 1988), engineering of acoustic pressure (Sojahrood et al., 2015), and use of the amplitude of the peaks/dips in inferring pressure (Li et al., 2018). However, advantages of a deep learning approach, in a passive pressure measurement system that is entirely acoustic by processing the echo signal, have been unexplored to our best knowledge. Here, we study if deep learning can effectively predict pressure from an ultrasound signal that is reflected from a deformable polymeric structure/sensor. To assess its success, we compare this performance with prediction of pressure that employs resonant frequency that has been common (Forsberg et al., 2005; Gong, Cabodi, & Porter, 2010; Ishihara et al., 1988; Li et al., 2018; Tremblay-Darveau et al., 2014). While our measurement setup and transponder/sensor differ from these reports in terms of its material or shape; our comparison, in principle, can elucidate the path toward in improving the read-out sensitivity of fully passive transponders/sensors that operate with ultrasound.

In this paper, we compare the utility of a deep ResNet-style network with four identity blocks (Chen et al., 2020) and a CNN regression model (LeNet Style LeCun et al., 1989) with two convolutional layers, two pooling layers, and two fully connected layers (Zhu et al., 2017). We compare the performance of these networks with a baseline network (fully connected network) that has been widely used by various investigators (Feng et al., 2020; Huang et al., 2019; Kossaifi et al., 2020; Paul & Munkvold, 2005). Furthermore, we assess the shift of resonant frequency in the echo signal reflected from a transponder made from Polydimethylsiloxane (PDMS), and estimate the corresponding accuracy, if this shift is used as the sole metric for prediction of the pressure.

2. Setup for acquisition of the dataset

Measurement of the acoustic response of acoustic resonators at various pressures is achieved using a specifically designed and fabricated pressure chamber (Fig. 1) and measurement test setup (Fig. 2). The setup includes a 3D printed pressure chamber (Fig. 1), an ultrasound pulser (Imaginant DSR 300; Fig. 2), an ultrasound transducer 10 MHz (Figs. 1, 2), an oscilloscope (Tektronix, Fig. 2) for data acquisition, a pressure sensor (Omega Engineering; Fig. 2), a digital pressure regulator (Equilibar; Fig. 2), a digital multimeter for reading pressure (Agilent 34450A; Fig. 2), and a digital power supply (E3641A, Fig. 2) to drive the regulator. The pressure chamber is fully enclosed while it is pressured using the regulator. The chamber itself is immersed in a tank of water (Fig. 2 bottom) with a water level controller to keep the height of water. Since the chamber is immersed in a large water tank, to account for the pressure added due to a column of water, a precision pressure transducer is attached to the chamber (See Fig. 1 bottom). The pressure transducer is attached to the pressure chamber (Fig. 1) for logging the data. The components are synchronized and controlled by a LabVIEW program running on a laptop. Approximately every 15 s the pressure is randomly set from 0 to 155 mmHg, and the Fast Fourier Transform (FFT) of the ultrasound's reflection are stored in a csv file. The oscilloscope averages the signal with 60 measurements before passing data to the laptop. The range of pressure is close to 0–180 mmHg, which is physiologically relevant to the intracardiac pressures that have been studied in other reports (Li et al., 2018). Here, the transponder compresses air encapsulated

in Polydimethylsiloxane (PDMS) microstructures. This structure is inspired by a variation of acoustic resonators that mimics the use of air bubbles in blood and has been widely studied (Ishihara et al., 1988; Li et al., 2018; Tremblay-Darveau et al., 2014), which enables us to have a well-controlled and repeatable design of acoustic transponders.

3. Datapoints and their storage

The reflection signal's FFT (a common feature for signal processing) is stored in ranges from 0 to 10 MHz with a resolution of 34.72 kHz. Each datapoint comprises a table of frequency (Hz) and signal's FFT (dB) that is stored in an excel file. For each datapoint, the time, date, setting pressure, and reading pressure are stored in the file name. To ensure that the signal is originated from the acoustic transponders, in the time domain, the signal reflected from the PDMS transponder is determined by its distance from the transducer. Subsequently the time window in the oscilloscope is manually set to the particular peak. This setting does not change during the data acquisition afterwards. Additionally, we amplified the signal using the setting (gain, damping, amplitude, and etc.) in the pulser such that we observe a resonant peak that is clearly shifting by the pressure. Next, a total of 3200 datapoints, at randomly chosen pressures, were collected and store using the aforementioned setup and protocol. Although, the data collection is attained using a single transducer and with the same geometrical constraints, the datapoints' feature vectors are not identical even at the same pressures as discussed later.

To visualize the effect of pressure on the signal's FFT, datapoints at pressures of 3, 60, 120, 145 mmHg are depicted in black, red, green, and yellow, respectively in Fig. 3(a). Here we observe a complex response of multiple dips are shifted due to the change of pressure. Furthermore, both the quality factor and the center frequencies are affected for all the dips. Here, in Fig. 3b, a certain range of frequencies (~7 MHz to 10 MHz) shows a significant shift of the resonant dips (shown by arrows). We note that multiple harmonics/dips make resolving the resonant frequencies challenging. This behavior could be attributed to multiple factors, such as: (1) hyperplastic materials (i.e., PDMS) can have an effective Young's modulus that nonlinearly changes with strain and therefore with pressure, (2) in elastomers a higher loss factor reduces the mechanical quality factor, and (3) large deformation in the elastomer enables a highly nonuniform structure and therefore results in many resonant peaks. The combination of these phenomena makes the reflected signal complex, as does the process of understanding the physical origin of the response complex. This complexity leads us to hypothesize that deep learning could be a suitable tool for determining pressure from a complex echo signal.

We utilized the setup for collecting 3200 datapoints from one sample over the course of one day. From an investigative perspective, it is essential to determine the diversity of the collected datapoints. It is advantageous to ensure that the data is diverse prior to using a learning algorithm. One metric to study the diversity of the datapoints is determining the minimum Euclidian distance between the feature vectors (FFT signals) for each pair of datapoints (Gong, Zhong, & Hu, 2019). To assess this metric, we calculated the Euclidian distance between every possible pair of datapoints and normalized it with the length of feature vectors (i.e., the total number of stored FFT for each data point; 288).

The calculation of the distances between feature vectors revealed (Fig. 4a) that the minimum normalized distance between all datapoint is nonzero 0.007 dB/n and its maximum is 0.046 dB/n. Moreover, there are 9 pairs of datapoints with pressure labels as close as 0.001 mmHg. Accordingly, the nonzero minimum distance confirms the presence of nonidentical feature vectors (FFT datapoints) as well as random noise in the datapoints. The histogram for the distance between all possible pairs of datapoints further illustrates a diverse set of training datapoints where all possible pairs of feature vectors are nonidentical (Fig. 4a). Observing the histogram for the pressure label distribution confirms a uniform distribution of pressures (Fig. 4b). Accordingly, the dataset can be spilt into training, validation, and test dataset without the repetition of identical datapoints in each set.

4. Neural network regressors and conventional method for calculation of pressure

A conventional method for estimation of pressure is measurement of the resonant frequencies. The relationship between the pressure and the resonant frequency at ~8.3 MHz (shown in Fig. 3b) for all datapoints is depicted in Fig. 5. Here we choose this peak because it shows a larger shift in frequency at varying pressure (in comparison with peak at ~7 MHz), and has a large quality factor (in comparison with the peak at 9.5 MHz). Since the frequency resolution is constant, increasing these two factors, in the absence of random error, can improve the accuracy of the pressure readout. We note that ideally one needs to study the underlying physics to find the ideal resonant peak, which is beyond the focus of this work.

To calculate the error bar, the pressures are divided into intervals of 2 mmHg, and all the pressures falling in each interval range are averaged. Subsequently the average and the related error bar are plotted. The plot here shows an almost linear relationship between pressure and frequency in the range of 0 to 100 mmHg. Assuming a linear relationship we have:

$$F_{resonance} = c_1 + c_2 P \tag{1}$$

where c_1, c_2 are constants, P is the pressure and F is the frequency. This equation results in the variation of measurement of pressure as follow:

$$\Delta P_{resonance} = \frac{\Delta F_{resonance}}{|\, c2 \,|} \tag{2}$$

Here $\Delta P_{resonance}$ denote uncertainty corresponding to calculation of pressure solely using the resonant frequency. Here, we note that the resolution for reading frequency imposed by the oscilloscope is $\Delta F_{resolution} = 34.727$ kHz and the error suggested by the empirical data in Fig. 1 is greater than ±100 kHz. Therefor the empirical data here suggests $\Delta F_{accuracy} > 100$ kHz and possible improvement may improve it to $\Delta F_{resolution} > 34$. Estimating $c_2 \sim 2.5$ kHz/mmHg results in an empirical error in measurement of $\Delta P_{resonance}$ greater than ±40 mmHg.

Subsequently, given the resolution of reading frequencies, a reasonable resolution for the pressure will become $\Delta P_{resonance} > 14$ mmHg.

The error in inferring the pressure, raises the question if the measurement test setup is providing sufficiently accurate results. Verification of the setup's measurement accuracy in reading pressure is done by comparing the transducers' accuracy and comparing the pressure readings from two different source. The transducers are attached to the chamber and the pressure regulator and have accuracy of 0.7 and ±0.25 mmHg respectively. These accuracies result in an expectation of random error better than 0.7 mmHg. To assess the possibility of systematic errors we compare the setting pressure in the pressure regulator (P_{set}) and the measured pressure (P_{measured}) that is carried out by the sensor attached to the pressure chamber. Fig. 6 compares the difference between these two pressures as a function of P_{set}. The positive differential pressure verifies that the P_{measured} is always greater than P_{set}. This is consistent with the fact that there exists a column of water above the sensor as well as the tubing attached to the pressure chamber. Furthermore, the comparison grows our confidence that systematic errors (if could not be accounted for) do not exceed ±1.5 mmHg since the maximum deviation of the two pressures is smaller than 3 mmHg. Finally, the small variation of the pressure difference at any P_{set} is limited to ±0.25 mmHg that can be seen as the thickness of the line in Fig. 6. This variation is attributed to the inherent inaccuracy of the transducer. Accordingly, Fig. 6 grows our confidence in using the measured pressure from the transducer attached to the pressure chamber. Overall, errors associated with the setup (Figs. 1, 2) is about two to three orders of magnitude smaller that the error in the prediction of pressure using the frequency shift.

Three regression models were employed that were inspired by the architectures of ResNet (Chen et al., 2020), CNN (LeNet), and a baseline fully connected network. The baseline network included four fully connected layers, including 64, 32, 4 and 1 neurons. The hidden layers have a ReLU activation function, and one dropout layer is included between the second and third layers. The LeNet style regression model included two blocks of 1D convolutional layers with 16 filters with *maxpooling* layers with a pool with the size of 2 and stride of 2. This layer was followed by fully connected layers with 200, 40, and 1 neurons. The fully connected layers have the activation function of ReLU, while the layer with 40 neurons features one dropout layer. The ResNet style regressor includes one dense block and four identity blocks (Chen et al., 2020). Each identity block included a dense layer, a dropout layer, and a batch normalization layer followed by the ReLU activation function.

We trained the regression networks on a training dataset of 2560 datapoints and a validation dataset of 320 datapoints. The remaining 320 datapoints were used for testing the chosen model. The batch size was 40 datapoints, the Adam optimizer was chosen, and the cost function was Mean Square Error (MSE). Each network was trained for 2000 epochs, and the model selection criterion was the lowest cross-validation cost function (Stone, 1974). In Fig. 7, training, and validation error/loss for the regressors are plotted. It is noted that the dropout layer avoids overfitting, and this is why the training loss is often larger than the validation loss.

Cross-validation is carried out for model selection (tuning hyperparameters) and evaluation of the performance. The approach was the hold-out cross-validation to reduce overfitting (Refaeilzadeh, Tang, & Liu, 2009; Reitermanova, 2010). For this purpose, the dataset was split (Reitermanova, 2010) into three subsets of 80% training, 10% validation, and 10% testing dataset. The validation dataset was used for model selection (i.e. termination of training) and choosing the hyperparameters values (dropout ratios). For this purpose, the training epoch was treated as a hyperparameter, and the model with the lowest validation loss was chosen among the first 2000 epochs (Reitermanova, 2010). Dropout ratio was also treated as a hyperparameter for each model (ResNet, Baseline and CNN regressor); and was manually chosen (in the range from 0 to 1) such that the validation loss is minimal. The test dataset (10%) was held out for the evaluation of the performance of the final models (Reitermanova, 2010) as reported in Table 1.

In training the models, the Adam optimizer's hyperparameters (epsilon, learning rate, and gradient clipping) remained constant. The dropout ratio for each type of regressor was manually chosen from a range from 0 to 1. The optimal dropout ratio was chosen such that the validation loss becomes minimal. In our experience, in the fully connected model, a small dropout ratio (ranging from 0 to 0.1) outperformed the models with higher drop out ratio value >0.1. In the ResNet style regressor, we did not observe a significant improvement between different values of dropout ratios (validation loss varying from 10 to 17 $mmHg^2$). In the CNN regressor, dropout ratios ranging from 0 to 0.5 were found to have a validation loss ranging from 7 to 11 $mmHg^2$. Adapting non-zero dropout ratios did not reduce the validation loss, greater than 20%, in comparison with a model without a dropout layer.

5. Performance

Using the criterion of the lowest cross-validation loss (Stone, 1974), models were selected. Subsequently, the test dataset was used for the evaluation of the three chosen models named baseline, Res-Net style and CNN regressors. The test dataset was used only once, which was in the end of the model section. Furthermore, the nonzero (L-2) minimum distance between the datapoints (Fig. 4a) ensured that the feature vectors in the validation/training datasets are not repeated in the test dataset. Subsequently, the performance of the baseline model, ResNet, and CNN regression models on the test datasets are compared in Fig. 8. In Fig. 8, the pressure predicted by the three models for the test feature vectors are plotted as a function of the ground truth pressure labels. As mentioned earlier the total number of 320 datapoints are present in the test dataset and this figure. In Fig. 8a,b the predicted pressure is plotted for a wide range of the actual pressure ranging from 3 to 158 mmHg. Here the baseline, Res-Net style, and CNN regressors are presented by horizontal blue line, vertical red line, and green circles respectively. Moreover the ideal prediction (ground truth) is presented by large grey circles. For comparison with a conventional pressure prediction method, error bars (grey long vertical lines) are shown (Eq. (2)). These error bar lines estimate the lower bound of error in the pressure prediction if one only uses the change of resonant frequencies at 8.3 MHz (Fig. 5 and Eq. (2)). We note that in practice these error bars are the best-case scenario since the pressure/frequency plot is not linear beyond 100 mmHg (Fig. 5). The regressors' average mean square error is evaluated for the training, validation, and test datasets in Table 1. Here the average mean square error for the

Baseline, ResNet-style, and CNN networks are presented. The accuracy (95% confidence) is calculated based on the MSE for the testing dataset and reported to be ±6, ±6, ±9 mmHg for the CNN, ResNet-Style, and baseline regressors, respectively. These error bars are significantly smaller than the uncertainty expected from the aforementioned conventional method for measurement of pressure (~>±40 mmHg). This comparison demonstrates that use of NN can be highly advantageous for calculation of pressure from the acoustic signal reflected from the pressure transducers/sensors.

The regression network's provides a reasonable level of accuracy (±6 mmHg) given that in intracardiac pressure measurement estimate, have a typical variation ranging from 1 to 4 mmHg (Abraham et al., 2011). This accuracy is also close to the reported accuracy of pressure measurement using backscattered acoustic signals (±2.5 mmHg Forsberg et al., 2005) in microbubbles. We note that the reported accuracy here does not outperform the best achievement in the reports (e.g. ±2.5 mmHg Forsberg et al., 2005). However, the success of these works is also attributed to optimizing the measurement tools, dimensions of the resonators, and mechanics/materials of these resonators (i.e., coating with protein or polymers), which are not the focus of this study. On the other hand, rather than optimizing all aspects of the acoustic transponder/sensors, we assess the utility of an algorithm that leverages neural networks. Our comparison demonstrates that utility of neural networks has potentials to improve the state-of-art accuracy of measurements using fully acoustic sensor/devices if it is combined with optimizing the transponders' materials/dimensions, the readout systems, or acoustic pressures.

6. Conclusion

Neural networks offer a complete method for analyzing complex data in the reflection from a fully acoustic transponder with stationary transducers. In our setup, they offered an accuracy of about 4% of the full range of pressure, in aqueous media, with a minimal need for the intervention of the user. They significantly outperform a conventional signal processing method that only considers the shift to a single resonant peak, in our experiment. Our work also suggests that both deep residual networks and convolution networks outperform fully connected networks for regression of the pressure. They also suggest the need for further studies on utilizing neural networks in inferring pressures from acoustic transponders/sensors in lossy environments and those with significant motions/misalignments.

Acknowledgments

Research reported in this publication was supported by the National Institute Of Biomedical Imaging And Bioengineering of the National Institutes of Health under Award Number R21EB030654. The content is solely the responsibility of the authors and does not necessarily represent the official views of the National Institutes of Health. S. Alaie also thank the department of mechanical & aerospace engineering and college of engineering at New Mexico State University for their support. The authors thank Hemanta Dulal for fabrication of the transponder and assisting in collection of data, Oscar Lara for generating the schematics, and Nathan Rydecki for assisting in fabrication of parts for the benchtop test setup.

Declaration of competing interest

S. Alaie and S. Al'Aref are among the coinventors in a patent application of WO2019152851A1 named "Acoustic transponders for wireless pressure monitoring using flexible acoustic resonators". The patent application pertains

the use acoustic transponders for measurement of pressure through the shift of the resonant frequencies rather than the use of Neural Networks. The authors have not received income related to this right or application. S.J.A. is supported by NIH 2R01 HL12766105 and 1R21 EB030654 and receives royalty fees from Elsevier.

Data availability

Data will be made available on request

References

Abraham WT, Adamson PB, Hasan A, Bourge RC, Pamboukian SV, Aaron MF, & Raval NY (2011). Safety and accuracy of a wireless pulmonary artery pressure monitoring system in patients with heart failure. American Heart Journal, 161(3), 558–566. [PubMed: 21392612]

Ahn JJ, Byun HW, Oh KJ, & Kim TY (2012). Using ridge regression with genetic algorithm to enhance real estate appraisal forecasting. Expert Systems with Applications, 39(9), 8369–8379.

Amendola S, Bianchi L, & Marrocco G (2015). Movement detection of human body segments: Passive radio-frequency identification and machine-learning technologies. IEEE Antennas and Propagation Magazine, 57(3), 23–37.

Chen D, Hu F, Nian G, & Yang T (2020). Deep residual learning for nonlinear regression. Entropy, 22(2), 193. [PubMed: 33285968]

Debourg E, Rifai A, Aubert H, Pons P, Augustyniak I, Knapkiewicz P, …, & Lavielle D (2014). Wireless passive high-doses radiation sensor. In Sensors, 2014 IEEE (pp. 1165–1168). IEEE.

Fairbank WM, & Scully MO (1977). A new noninvasive technique for cardiac pressure measurement: resonant scattering of ultrasound from bubbles. IEEE Transactions on Biomedical Engineering, (2), 107–110. [PubMed: 892812]

Feng X, Ma G, Su S-F, Huang C, Boswell MK, & Xue P (2020). A multi-layer perceptron approach for accelerated wave forecasting in Lake Michigan. Ocean Engineering, 211, Article 107526.

Forsberg F, Liu J-B, Shi WT, Furuse J, Shimizu M, & Goldberg BB (2005). In vivo pressure estimation using subharmonic contrast microbubble signals: Proof of concept. IEEE Transactions on Ultrasonics, Ferroelectrics and Frequency Control, 52(4), 581–583. [PubMed: 16060506]

Gong Y, Cabodi M, & Porter T (2010). Pressure-dependent resonance frequency for lipid-coated microbubbles at low acoustic pressures. In 2010 IEEE international ultrasonics symposium (pp. 1932–1935). IEEE.

Gong Z, Zhong P, & Hu W (2019). Diversity in machine learning. IEEE Access, 7, 64323–64350.

Haile MA, Zhu E, Hsu C, & Bradley N (2020). Deep machine learning for detection of acoustic wave reflections. Structural Health Monitoring, 19(5), 1340–1350.

Hennig A, & vom Bögel G (2010). A data transmission technique for passive sensor-transponders in medicine. In 2010 IEEE international conference on RFID (IEEE RFID 2010) (pp. 215–222). IEEE.

Huang X, Gao L, Crosbie RS, Zhang N, Fu G, & Doble R (2019). Groundwater recharge prediction using linear regression, multi-layer perception network, and deep learning. Water, 11(9), 1879.

Ishihara K, Kitabatake A, Tanouchi J, Fujii K, Uematsu M, Yoshida Y, …, & Shirae K (1988). New approach to noninvasive manometry based on pressure dependent resonant shift of elastic microcapsules in ultrasonic frequency characteristics. Japanese Journal of Applied Physics, 27(S1), 125.

Jiang H, Carter NM, Zareei A, Nejati S, Waimin JF, Chittiboyina S, …, & Goergen CJ (2020). A wireless implantable strain sensing scheme using ultrasound imaging of highly stretchable zinc oxide/poly dimethylacrylamide nanocomposite hydrogel. ACS Appl Bio Mater., 3(7), 4012–4024.

Kohler M, & Langer S (2021). On the rate of convergence of fully connected deep neural network regression estimates. The Annals of Statistics, 49(4), 2231–2249.

Kossaifi J, Lipton ZC, Kolbeinsson A, Khanna A, Furlanello T, & Anandkumar A (2020). Tensor regression networks. Journal of Machine Learning Research, 21, 1–21. [PubMed: 34305477]

Lafci B, Merčep E, Morscher S, Deán-Ben XL, & Razansky D (2020). Deep learning for automatic segmentation of hybrid optoacoustic ultrasound (OPUS) images. IEEE Transactions on Ultrasonics, Ferroelectrics and Frequency Control, 68(3), 688–696.

LeCun Y, Boser B, Denker JS, Henderson D, Howard RE, Hubbard W, & Jackel LD (1989). Backpropagation applied to handwritten zip code recognition. Neural Computation, 1(4), 541–551.

Li F, Li D, & Yan F (2018). Improvement of detection sensitivity of microbubbles as sensors to detect ambient pressure. Sensors, 18(12), 4083. [PubMed: 30469461]

Lin J-H, & Kao Y-H (2008). Wireless temperature sensing using a passive RFID tag with film bulk acoustic resonator. In 2008 IEEE ultrasonics symposium (pp. 2209–2212). IEEE.

Luijten B, Cohen R, de Bruijn FJ, Schmeitz HA, Mischi M, Eldar YC, & van Sloun RJ (2019). Deep learning for fast adaptive beamforming. In ICASSP 2019-2019 IEEE international conference on acoustics, speech and signal processing (pp. 1333–1337). IEEE.

Martínez-Martínez JJ, Galindo-Romera G, & Herraiz-Martínez FJ (2017). Design of a low-cost wireless reader for an electromagnetic passive temperature sensor. In 2017 IEEE international symposium on antennas and propagation & USNC/URSI national radio science meeting (pp. 2503–2504). IEEE.

Medak D, Posilović L, Subašić M, Budimir M, & Lončarić S (2022). DefectDet: A deep learning architecture for detection of defects with extreme aspect ratios in ultrasonic images. Neurocomputing, 473, 107–115.

Nguyen TT, Fernandes LAL, & Häfliger P (2014). An energy-efficient implantable transponder for biomedical piezo-resistance pressure sensors. IEEE Sensors Journal, 14(6), 1836–1843.

Pandey M, Zakwan M, Sharma P, & Ahmad Z (2020). Multiple linear regression and genetic algorithm approaches to predict temporal scour depth near circular pier in non-cohesive sediment. ISH Journal of Hydraulic Engineering, 26(1), 96–103.

Paul P, & Munkvold G (2005). Regression and artificial neural network modeling for the prediction of gray leaf spot of maize. Phytopathology, 95(4), 388–396. [PubMed: 18943041]

Provencal E, & Laperrière L (2021). Identification of weld geometry from ultrasound scan data using deep learning. Procedia CIRP, 104, 122–127.

Pyle RJ, Bevan RL, Hughes RR, Rachev RK, Ali AAS, & Wilcox PD (2020). Deep learning for ultrasonic crack characterization in nde. IEEE Transactions on Ultrasonics, Ferroelectrics and Frequency Control, 68(5), 1854–1865.

Raju R, & Bridges GE (2021). Radar cross section-based chipless tag with built-in reference for relative humidity monitoring of packaged food commodities. IEEE Sensors Journal, 21(17), 18773–18780.

Raju R, & Bridges GE (2022). A compact wireless passive harmonic sensor for ammonia sensing in packaged food. IEEE Sensors Letters, 6(4), 1–4.

Refaeilzadeh P, Tang L, & Liu H (2009). Cross-validation. Encyclopedia of Database Systems, 5, 532–538.

Reitermanova Z (2010). Data splitting. In WDS, *Vol.* 10 (pp. 31–36). Matfyzpress Prague.

Schimetta G, Dollinger F, Scholl G, & Weigel R (2001). Optimized design and fabrication of a wireless pressure and temperature sensor unit based on SAW transponder technology. In 2001 IEEE MTT-S international microwave sympsoium digest (cat. no. 01CH37157), *Vol.* 1 (pp. 355–358). IEEE.

Shi G, He Y, Gu L, & Jiao J (2021). Industry 4.0-oriented chipless RFID backscatter signal variable polarization amplitude deep learning coding. Wireless Communications and Mobile Computing, 2021, 1–11. [PubMed: 35573891]

Sojahrood AJ, Falou O, Earl R, Karshafian R, & Kolios MC (2015). Influence of the pressure-dependent resonance frequency on the bifurcation structure and backscattered pressure of ultrasound contrast agents: a numerical investigation. Nonlinear Dynamics, 80, 889–904.

Stone M (1974). Cross-validatory choice and assessment of statistical predictions. Journal of the Royal Statistical Society. Series B. Statistical Methodology, 36(2), 111–133.

Tremblay-Darveau C, Williams R, & Burns PN (2014). Measuring absolute blood pressure using microbubbles. Ultrasound in Medicine & Biology, 40(4), 775–787. 10.1016/j.ultrasmedbio.2013.10.017. [PubMed: 24433747]

Villa-Gonzalez F, Bhattacharyya R, & Sarma S (2021). Single and bulk identification of plastics in the recycling chain using chipless RFID tags. In 2021 IEEE international conference on RFID (pp. 1–8). IEEE.

Ye J, Ito S, & Toyama N (2018). Computerized ultrasonic imaging inspection: From shallow to deep learning. Sensors, 18(11), 3820. [PubMed: 30405086]

Zhang G-M, & Harvey DM (2012). Contemporary ultrasonic signal processing approaches for nondestructive evaluation of multilayered structures. Nondestructive Testing and Evaluation, 27(1), 1–27.

Zhao A, Sunny AI, Li L, & Wang T (2022). Machine learning-based structural health monitoring using RFID for harsh environmental conditions. Electronics, 11(11), 1740.

Zhou N, Pierre JW, & Trudnowski D (2011). A stepwise regression method for estimating dominant electromechanical modes. IEEE Transactions on Power Systems, 27(2), 1051–1059.

Zhu A, Li X, Mo Z, & Wu R (2017). Wind power prediction based on a convolutional neural network. In 2017 international conference on circuits, devices and systems (pp. 131–135). IEEE.

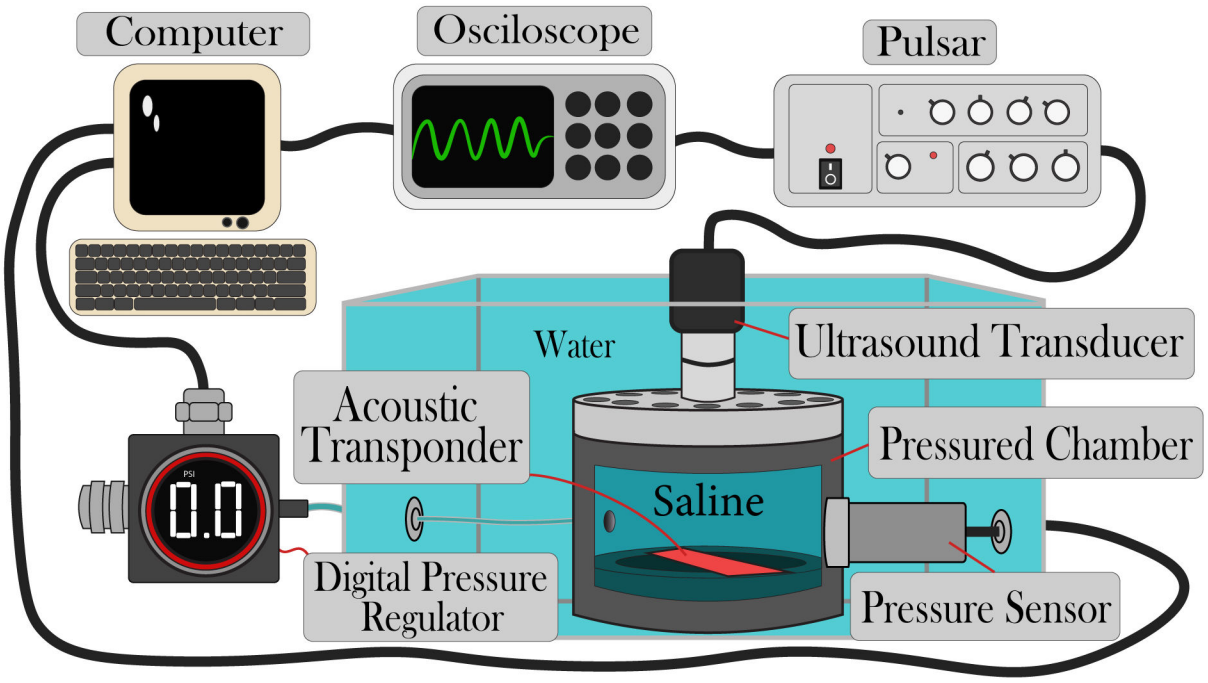

Fig. 1.

An experimental setup stores the ultrasound reflection signal from acoustic resonators inside a pressure chamber at randomly chosen pressures. The setup includes a pressure regulator, a pressure chamber, ultrasound transducer, oscilloscope, and a computer.

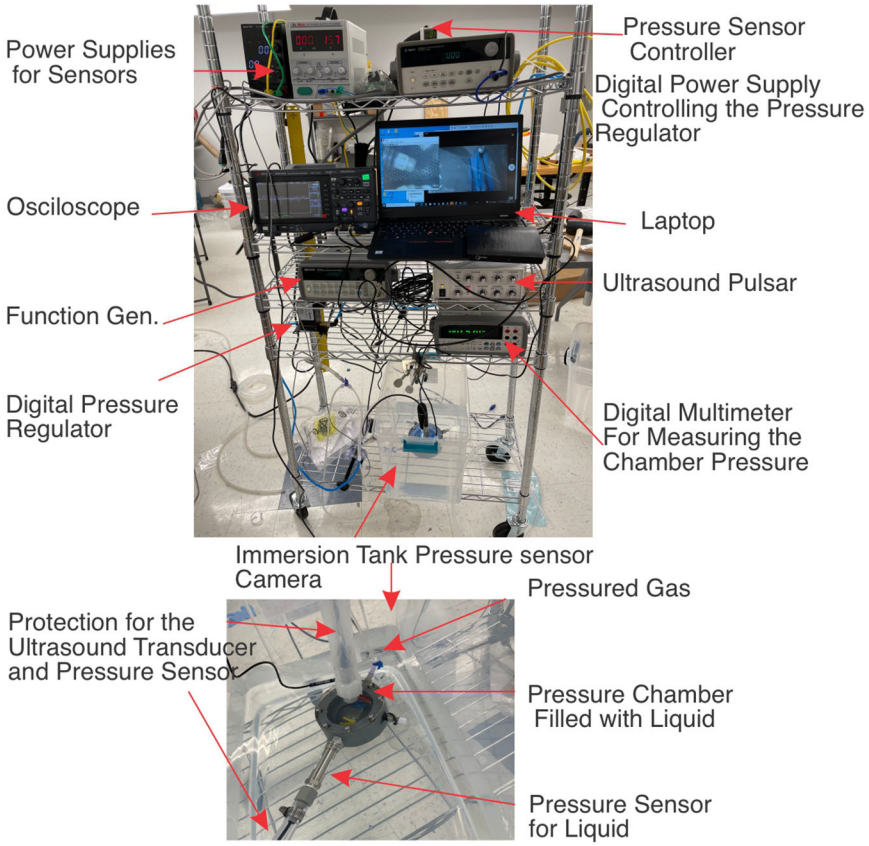

Fig. 2.

A measurement test setup for precision characterization film-like resonator's acoustic properties at various pressures.

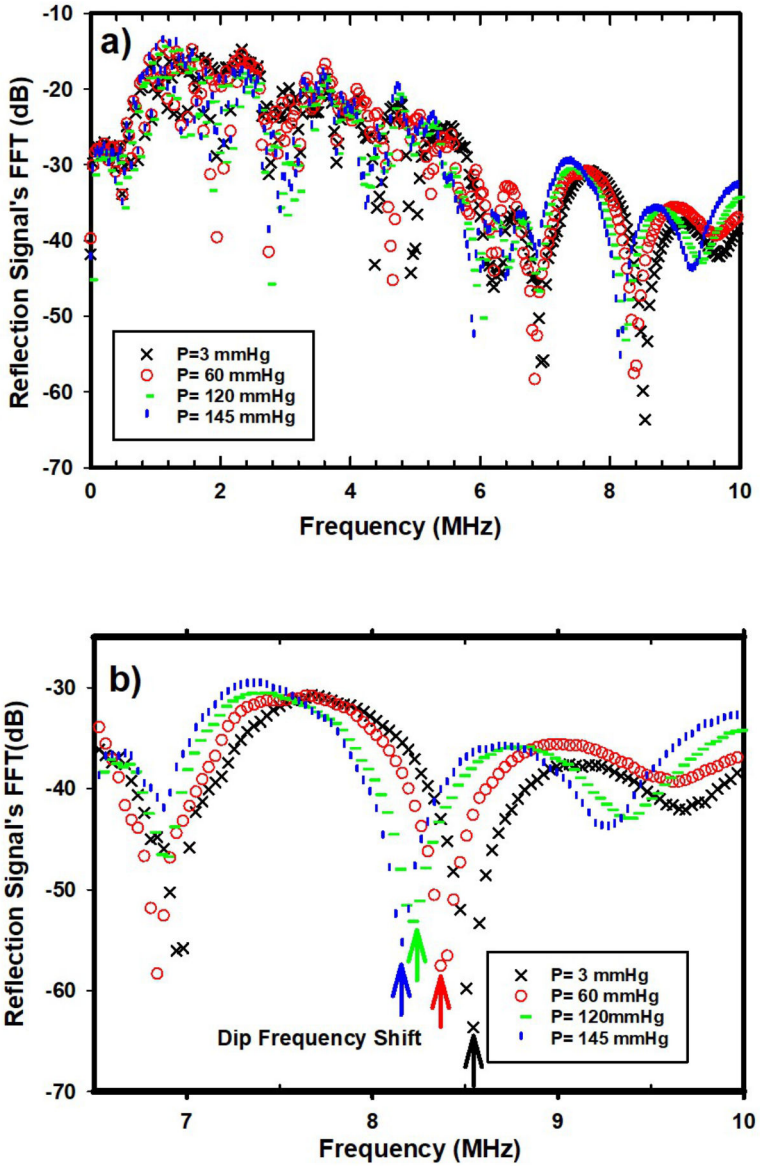

Fig. 3.

The FFT of the ultrasound reflection (a) dips significantly shift by the change in pressure (3, 60, 120, and 145 mmHg), (b) the shift of the resonant frequency as a result of changes in pressure is highlighted by arrows (dip ~8.5 MHz and 9.5 MHz). .

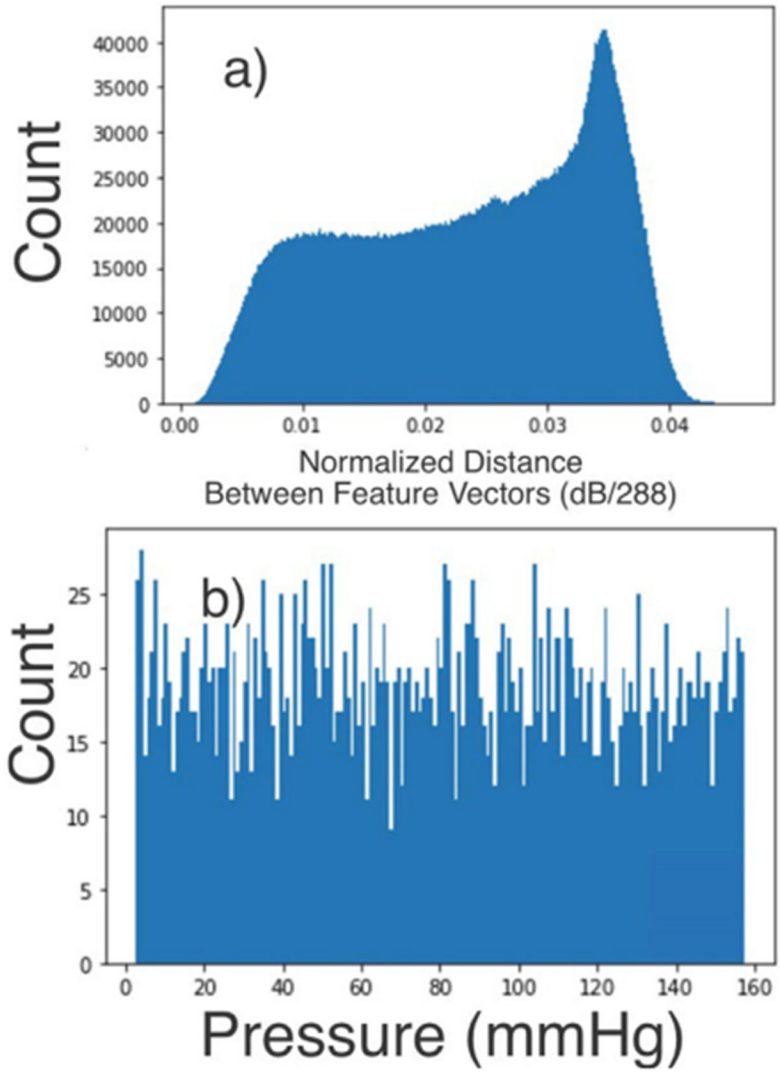

Fig. 4.

(a) The histogram for the normalized Euclidean distance between every possible pair of feature vectors shows that none of the datapoints are identical. (b) the histogram for the measured pressure ranges from 3 to 158 mmHg, which shows almost a uniform distribution of pressure.

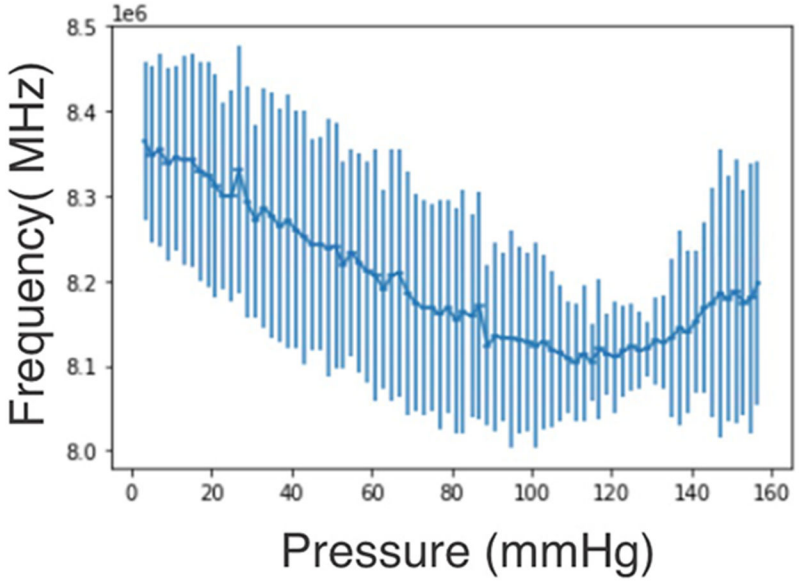

Fig. 5.

The center of the frequency dip in the FFT of the ultrasound reflection signal (referring to the center frequency of the dip in Fig. 3b), significantly changes with the change of pressure. The error bars are calculated based on the standard deviation of the measurements (center frequency of dips at various pressures) that fall within each interval of pressures.

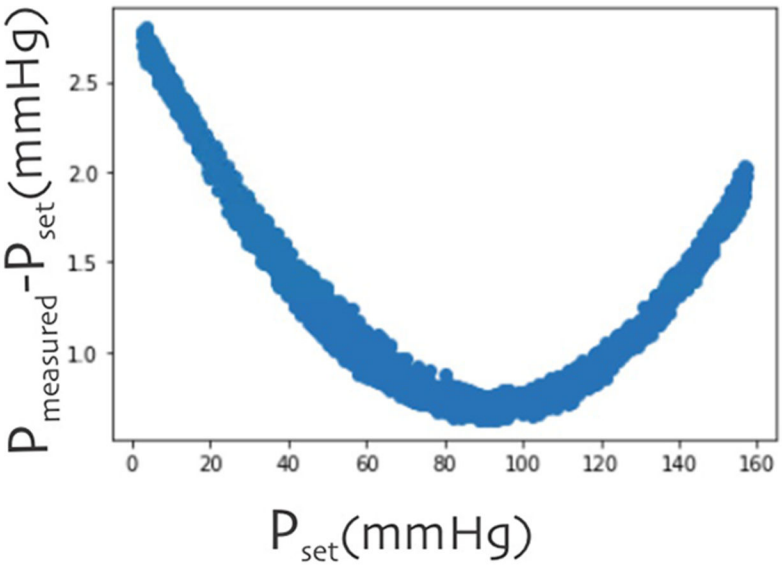

Fig. 6.

The pressure difference between the transducer attached to the pressure chamber ($P_{measured}$) and that of the pressure regulator (P_{set}) as a function of the setting pressure (at the pressure regulator; P_{set}). The small variation is attributed to the water column on top of the transducer and the noise is attributed to the inherent inaccuracy of the transducer.

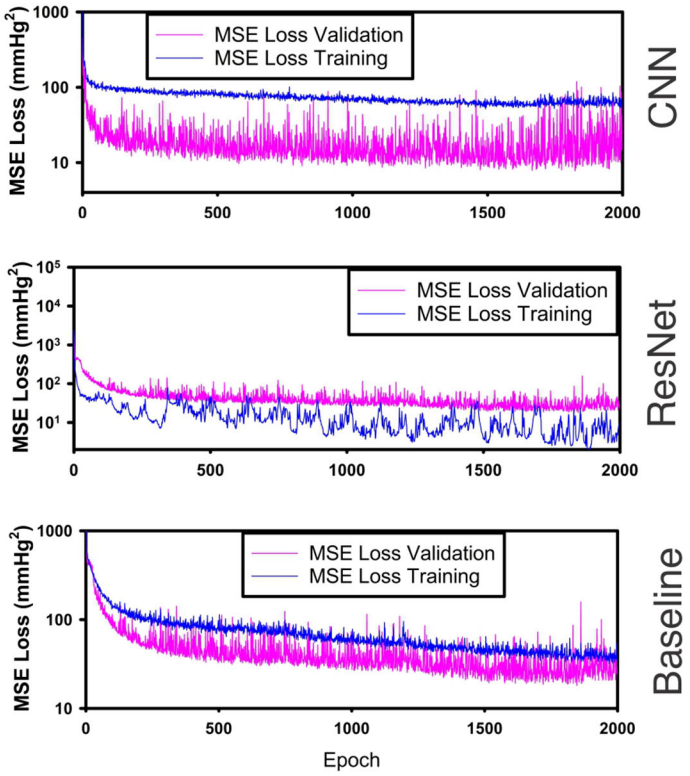

Fig. 7.

Training and validation loss (average Mean Square Error) for CNN (top), ResNet style (middle), and baseline regressors (bottom).

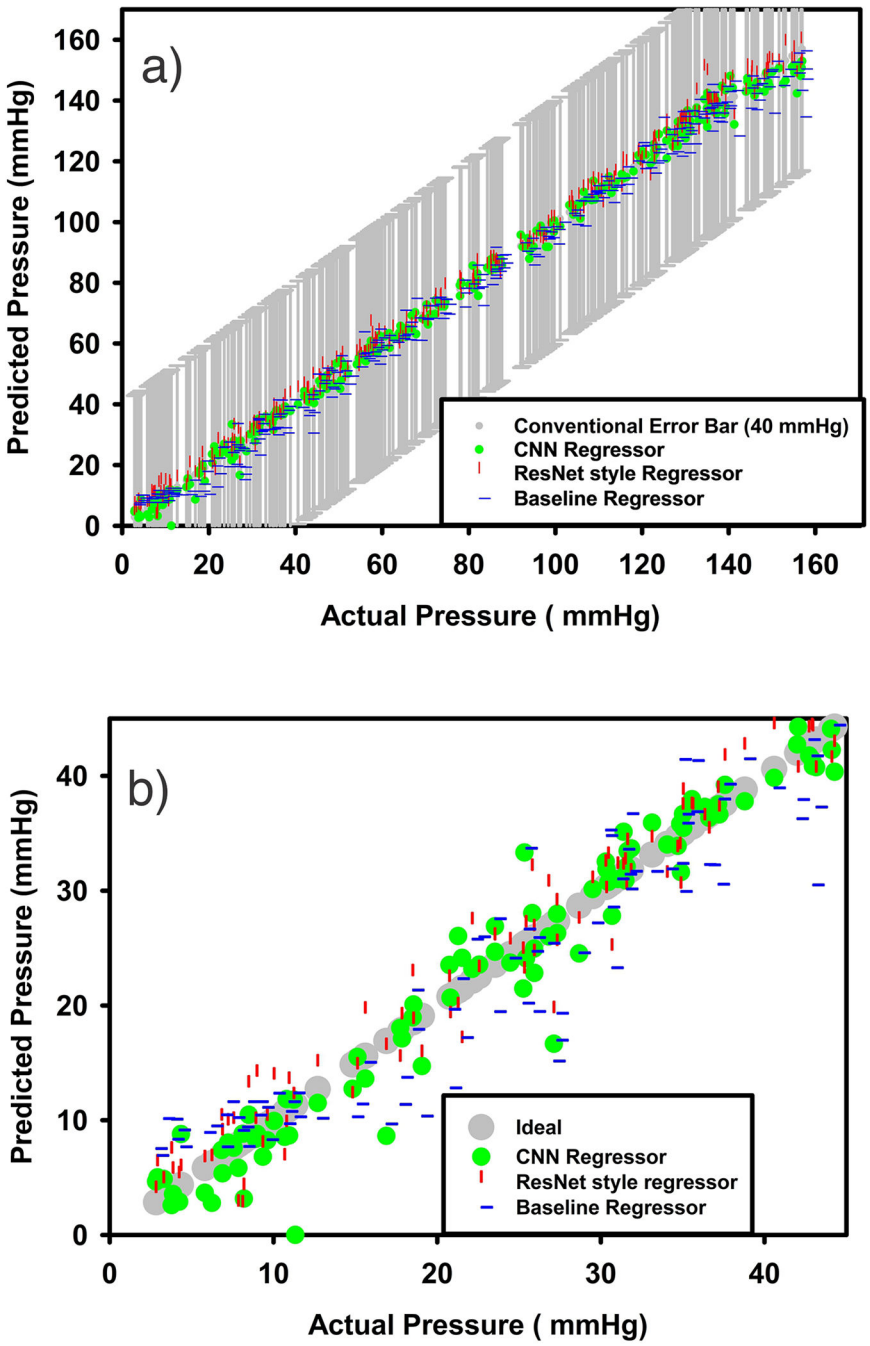

Fig. 8.

Predicted data as a function of the actual pressure in the test dataset plotted for CNN, Resnet-Style, and a baseline regressor. (a) The behavior is following a line in a wide range from 3 to 158 mmHg for all three models. The error bar shows the minimum error for prediction of pressure, if only the shift of the resonant frequency is considered based on Fig. 5. (b) At lower pressure the deviation from a linear relationship is more consequential for all three models because of the large percentage of error.

Table 1:

The performance of three networks, named baseline ResNet-Style and CNN regressors, on the training (80%), test (10%), and validation (10%) dataset. The test dataset was used only for evaluation of the selected model while the validation dataset was used for the model selection and choosing hyperparameters (10%). The reported losses are associated with the same hyperparameters for each type of regressor.

Architecture	Training MSE	Validation MSE	Test MSE	Accuracy (95%)
Baseline DenseNet	17 ($mmHg^2$)	19 ($mmHg^2$)	19 ($mmHg^2$)	± 9 mmHg
ResNet Style	7 ($mmHg^2$)	10 ($mmHg^2$)	10 ($mmHg^2$)	± 6 mmHg
CNN Style	4 ($mmHg^2$)	8 ($mmHg^2$)	9($mmHg^2$)	± 6 mmHg
Resonant Frequency Shift[a]				> ±40 mmHg

[a]If the center of dip frequency at 8.5 MHz is used for inferring pressure (Figs. 3b, 5). Measurement of pressures beyond 100 mmHg results in a greater uncertainty (Fig. 5) due to the nonlinearity.